REMOTE SENSING OF MARINE PARTICLE PROPERTIES USING SHIPBOARD OCEANOGRAPHIC LIDAR

Author: Brian Collister
Advisor: Dr. Richard Zimmerman
Department of Ocean and Earth Sciences; Old Dominion University; Norfolk, VA, 23517

Abstract

Oceanographic lidar has the potential to revolutionize our understanding of ocean ecosystems by providing a means to remotely measure the vertical distribution of biomass in the upper ocean. In addition to providing information on material concentration, the polarization state of the return signal contains information on bulk properties (shape, size, and composition) of the particle population that could be used to better parameterize the role of marine ecosystems in Earth's climate. In this study, we explored the response of the lidar depolarization ratio (δ) to changes in particle type and particle density, using a bio-optical model in conjunction with measurements of lidar depolarization, in-water optical properties, and polarized light scattering by marine particles. Laboratory measurements suggest that δ varies with particle composition and morphology, but that the complexity of its behavior may limit the utility of δ for measuring bulk particle properties. The relative contribution of particles to total backscattering was the strongest driver of changes in δ, with differences in forward scattering depolarization playing a minor role in driving δ. These results suggest that δ may be less useful as a metric for particle type, but can likely provide information on the total scattering coefficient from its behavior with depth.

Introduction

Ocean color remote sensing provides the primary means for measuring phytoplankton distributions across the surface ocean[1]. However, these techniques are limited in scope by their reliance on the sun as a passive radiation source; measurements represent a daytime, surface-weighted average over the ocean's first optical depth, missing deep phytoplankton populations and providing no information on their vertical structure. This "missing" vertical information leads to substantial errors in estimates of primary production, as the vertical distribution of biomass plays a key role in determining its exposure to factors controlling growth[2]. Oceanographic lidar offers to fill this observational gap by providing a means to measure the vertical distribution of marine ecosystems remotely via the range-resolved detection of a backscattered laser pulse. The ability to penetrate the air-sea interface and provide ranging information is unique to ocean lidar, making it the only remote sensing technique with potential to meet requirements for global, three-dimensional measurements of ocean ecosystems.

In addition to revealing the vertical structure of particle concentration in the upper ocean, oceanographic lidar can provide information on the intensive (concentration independent) properties of the particle assemblage by analysis of the polarization state of the backscattered pulse. The typical application of this technique involves the emission of a linearly polarized pulse, and detection of the parallel and orthogonal polarization components of the backscattered return. In the single scattering domain, the ratio of the cross- and co-polarized returns [the linear depolarization ratio (δ)] can be used to estimate the 2,2-element of the normalized scattering matrix in the exact backscattering direction [$\mathbf{M}_{22}(\pi)$]:

$$\mathbf{M}_{22}(\pi) = \frac{1-\delta}{1+\delta} \qquad \text{Eq. 1}$$

an inherent optical property (IOP) that exhibits dependencies on the shape, size, and composition of the particle population[3,4]. Relationships established between $\mathbf{M}_{22}(\pi)$ and these intensive particle properties then provide the framework for interpreting lidar measurements of δ in the context of bulk particle properties. Beyond the single scattering domain, multiple scattering causes an increase in δ with optical depth, at a rate that depends on the magnitude of the scattering coefficient (b), the shape of $\mathbf{M}_{22}$ at near-forward angles, and the geometry of the lidar system[5,6]. Thus, multiple scattering gives δ additional sensitivities to the intensive and extensive properties of the particle assemblage that must be accounted for when using δ to estimate bulk particle properties.

Several recent oceanographic lidar studies suggest that the polarization lidar technique could be used to derive the intensive properties of aquatic particles[7-9]. Advancement of this capability would improve our ability to investigate the dynamics of particle mediated processes in the ocean, and to represent particles with distinct ecological roles in models of ocean biogeochemistry. However, these studies have been mostly empirical in nature, failing to advance the mechanistic framework required to link changes in δ to changes in the nature of aquatic particle populations. Progress toward this framework has been historically limited by two major knowledge gaps: 1) a lack of information on the polarized light scattering properties of marine particles, and 2) an incomplete understanding of the multiple scattering influence on measurements of δ. The goal of this study was to improve our ability to interpret polarized oceanographic lidar signals, by exploring the separate contributions of single and multiple scattering to oceanographic lidar depolarization measurements. We accomplished this by parameterizing a bio-optical model with laboratory measurements of $\mathbf{M}_{22}$ and field measurements of in-water IOPs to simulates the dept dependence of lidar depolarization in the context of a field deployment of a shipboard oceanographic lidar.

Methods

Lidar Dataset

To explore the primary factors contributing to the oceanographic lidar depolarization ratio, we used a dataset of coincident *in situ* IOP and polarized oceanographic lidar measurements that we collected during the Coccomix research expedition to the Gulf of Maine and North Atlantic[7]. For the duration of the research cruise, the lidar depolarization ratio δ was measured at a depth of 6.5 m. The particulate scattering coefficient (b_p) was measured continuously at the surface using a WET Labs *ac*-9 spectrophotometer, and the total scattering coefficient (b) was calculated as $b = b_p + b_w$, where b_w is the scattering coefficient for seawater calculated from measurements of temperature and salinity[10]. The total particulate backscattering coefficient (b_{bp}) was measured using a Wyatt DAWN light scattering detector, and the acid labile backscattering coefficient was measured by difference from b_{bp} measured from a bulk sample and a sample that was acidified to dissolve all particulate calcite. The total backscattering coefficient was calculated as $b_b = b_{bp} + b_{bw}$, where b_{bw} was also calculated from temperature and salinity[10].

Scattering Materials

To characterize the variability of $\mathbf{M}_{22}$ in marine particle populations and to parameterize the lidar bio-optical model, the near-backwards lidar depolarization ratio was measured for several compositionally and morphologically distinct marine particle populations. We prepared three mono-specific phytoplankton cultures: a calcifying

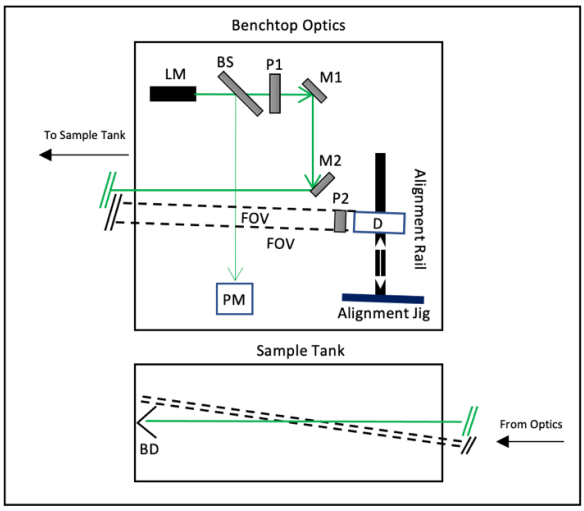

Fig. 1 Plan view of optical configuration used for the depolarization measurements. a) Source optics consisted of a 532 nm laser module (LM), beamsplitter (BS), linear polarizer (P1), and two beam-steering mirrors (M1 and M2). A detector module (D) was mounted to an optical rail, allowing it to be translated (white arrows) between an alignment jig (blue bar) and the measurement position. A reference detector (PM) sampled the split beam. The beam path is shown in green and the FOV is shown by dashed black lines. b) The beam and FOV overlapped in the center of the sample tank before the beam was terminated by a beam dump (BD) positioned at the rear of the tank. Drawings not to scale; angles exaggerated for illustration purposes.

strain of the coccolithophore *Emiliania huxleyi*, a centric diatom *Thalassiosira weissflogii*, and a marine cyanobacteria *Synechococcus sp*. Cultures were grown at 20°C with a 13:11 hour light/dark cycle and 60 µmol photons m^{-2} s^{-1} incident photosynthetically available radiation. *Emiliania huxleyi* was grown in L1-Si/25 media to promote coccolith production; *Thalassiosira* and *Synechococcus* were grown in L1 media. Cultures were maintained in the exponential growth phase and were harvested for measurement in the late exponential phase. Cell and coccolith counts were made using a Neubauer counting chamber. Calcified cells and detached coccoliths were identified by viewing samples through cross-polarized light.

In addition to phytoplankton cultures, an analog for suspended coccoliths was prepared from reagent-grade powdered calcite (J.T. Baker). Calcite powder was ground using a mortar and pestle and sifted through a 30 µm sieve prior to being suspended in calcium-saturated ultra-pure water (Barnstead Nanopure®; 18 MΩ). The particle size distribution of the stock calcite suspension was further reduced to a median particle diameter of ~2 µm using a settling column.

The spectral beam-attenuation coefficient [$c_{pg}(\lambda)$] for each stock scattering solution was measured using a benchtop spectrophotometer with a 1 cm cuvette that was blanked with ultrapure water (Shimadzu 2700i). For *E. huxleyi*, c_{pg} was measured again after acidification (c_{pg}^{acid}) of the sample, and the acid labile component of each measurement was calculated by difference ($c_{pg}' = c_{pg} - c_{pg}^{acid}$).

Depolarization Measurements

Depolarization measurements were made in the near backward direction (178.5°) using a custom benchtop laboratory optical assembly (c.f. Fig. 1). The light source consisted of a 532 nm collimated diode-pumped solid state laser module (LM; Thorlabs CPS532; 4.5 nW; 3.55 mm diameter; 0.5 mrad divergence) aligned such that the major polarization axis was parallel to the benchtop reference plane. A fraction of the beam was diverted by a beam sampler (BS), positioned directly after the laser, to a power meter (PM; Thorlabs S130C) that served as a reference detector (PM; Fig. 1). A linear polarizer (P1; Thorlabs LPVISE2X2; 500:1 extinction ratio) positioned after the beam sampler was used to clean up the source polarization, and a pair of beam steering mirrors (M1 and M2) were used to orient the beam to be orthogonal to the face of a glass aquarium that served as a

sample cuvette. A beam dump positioned at the rear of the tank prevented specular reflection of the beam from the back wall.

The receiver assembly (D) consisted of a collecting lens (Thorlabs LA1608; f=75.0 mm), a 0.8 mm aperture positioned at the focal point of the lens, a 532 nm bandpass filter (Semrock LL01-532-12.5) to reject ambient light, and a photomultiplier tube (PMT; Hamamatsu H10721-20) detector. The full-angle receiver field of view (FOV) was constrained by the collection optics to be <0.5 mrad. A linear polarizer (P2; Thorlabs LPVISE2X2; Extinction Ratio = 500:1) fixed to an indexed rotation mount was positioned in front of the detector assembly to serve as a polarization analyzer. A multi-channel power supply (Keithley 2231A-30-3) provided a 5V power source to the PMT module as well as a 0.5-1.1V source for controlling the PMT gain. The PMT signal voltage was averaged over 10 seconds for each measurement, and was recorded using an oscilloscope (Tektronix TDS2024C).

The detector was aligned to the scattering volume as follows. Vertical alignment was achieved by aiming the assembly at the spot projected by the laser on the front glass of the tank and adjusting its height to maximize the signal recorded by the PMT. The detector assembly was then set to view at an in-air angle of 178° (178.5° in-water) from the source beam using an alignment jig. Finally, the detector was aligned in the horizontal by temporarily placing a diffuse white target in the beam path at the center of the tank, and translating the detector assembly along a rail mounted behind M2 until the detector viewed the laser spot projected on the alignment target and the signal recorded by the PMT was maximized. Correct alignment was confirmed by viewing the image of the alignment spot projected by the collection lens onto the receiver aperture.

Depolarization measurements were made by serial additions of scattering material to the aquarium filled with a background of filtered water. For the laboratory calcite and diatomaceous earth measurements, the background consisted of ultrapure water (Barnstead Nanopure®; 18 MΩ). To prevent dissolution during the calcite measurement, the water was amended with calcium chloride and sodium bicarbonate, and buffered with sodium hydroxide to a pH of 8.2. For all culture measurements, artificial seawater (Instant Ocean®; salinity = 32) filtered through a 0.2 μm filter cartridge (Pall AcroPak 500) was used in place of pure water to prevent osmotic cell lysis. Measurements of the co- and cross-polarized returns were made for the background water ($S_{\parallel}^{\text{blank}}$ and $S_{\perp}^{\text{blank}}$) and each sample addition ($S_{\parallel}^{\text{sample}}$ and $S_{\perp}^{\text{sample}}$) by rotating P2 between the co- and cross-polarized orientations. PMT dark counts were measured by obscuring the collection optics and were subtracted from each measurement of $S_{\parallel}$ and $S_{\perp}$. The near-backwards depolarization ratio (δ) was then calculated as:

$$\delta = \frac{S_{\perp}^{\text{sample}} - S_{\perp}^{\text{blank}}}{S_{\parallel}^{\text{sample}} - S_{\parallel}^{\text{blank}}} \qquad \text{Eq. 2}$$

To ensure that measurements were made within the single scattering domain, δ was calculated only for regions of the serial addition where the total return signal ($S = S_{\parallel} + S_{\perp}$) increased approximately linearly with sample concentration and where δ was independent of particle concentration. Values of δ were averaged over the single scattering domain of the measurement, and standard errors were calculated to estimate measurement uncertainty.

For the *E. huxleyi* culture, δ was further partitioned into an acid labile component composed of attached and detached coccoliths (δ_{PIC}) and a component composed of un-plated cells (δ_{n}). This was accomplished at the end of the serial addition by adjusting the pH of the sample with glacial

acetic acid (pH = 5.5) to dissolve the calcite and measuring the change in δ and S. δ_n and S_n then represented the post-acidification values of δ and S, and δ_{PIC} was calculated by assuming a linear contribution of δ_{PIC} and δ_n to δ that was proportional to the contribution of each material to S:

$$\delta = \frac{\delta_{PIC} S_{PIC} + \delta_n S_n}{S} \quad \text{Eq. 3}$$

For these measurements, standard additions were continued beyond the initial acidification while maintaining a pH of 5.5 to confirm that measurements remained within the single scattering domain.

Model Framework

A bio-optical model was constructed to separate the contributions of single and multiple scattering to lidar measurements of δ. The model was based on an analytical solution to the lidar radiative transfer equation that uses the small-angle approximation to solve for the vertical distribution of energy and the polarization characteristics of a backscattered laser pulse. For an initially linearly polarized pulse, the depth (z) dependent solution for the degree of linear polarization (*DoLP*) takes the form:

$$DoLP(z) = \mathbf{M}_{22}(\pi)\exp(-2\phi bz) \quad \text{Eq. 4}$$

where $\mathbf{M}_{22}(\pi)$ represents the 180-degree, normalized 2,2 scattering matrix element for whole seawater and ϕ is a depolarization factor that controls the exponential decay of *DoLP* with scattering optical depth (bz) due to multiple forward scattering. $\mathbf{M}_{22}(\pi)$ can be deconstructed into contributions from m scattering components as:

$$\mathbf{M}_{22}(\pi) = \sum_{n=1}^{m} \mathbf{M}_{22}^{n}(\pi) \frac{\beta_n(\pi)}{\beta(\pi)} \quad \text{Eq. 5}$$

where $\mathbf{M}_{22}^{n}(\pi)$ is the normalized 2,2 scattering matrix element for component n, $\beta_n(\pi)$ is the volume scattering by n at 180-degrees, and $\beta(\pi)$ is the volume scattering of the bulk medium at 180-degree. The forward scattering depolarization parameter can be deconstructed in a similar manner as:

$$\phi = \sum_{n=1}^{m} \phi_n \frac{b_n}{b} \quad \text{Eq. 6}$$

where ϕ^n and b_n are the depolarization factor and scattering coefficient for component n.

$\mathbf{M}_{22}(\pi)$ was parameterized by assuming three distinct scattering populations, acid-labile particles [$\mathbf{M}_{22}^{PIC}(\pi)$], non-acid labile particles [$\mathbf{M}_{22}^{POC}(\pi)$], and seawater [$\mathbf{M}_{22}^{w}(\pi)$]. Subbing these into Eq. 4 gives:

$$\mathbf{M}_{22}(\pi) = \quad \text{Eq. 7}$$
$$\frac{\beta(\pi)}{2\pi}\left[\mathbf{M}_{22}^{PIC}(\pi)\frac{b_b'}{\chi_{PIC}(\pi)} + \mathbf{M}_{22}^{POC}(\pi)\frac{b_{bp}-b_b'}{\chi_{POC}(\pi)} + \mathbf{M}_{22}^{w}(\pi)\frac{b_{bw}}{\chi_w(\pi)}\right]$$

where the $\chi(\pi)$ factors convert between total hemispherical backscatter and 180-degree backscatter for the acid labile, non-acid labile, and seawater components respectively. ϕ was parameterized for these three components using Eq. 6:

$$\phi = \phi_{PIC}\frac{b_{PIC}}{b} + \phi_{POC}\frac{b_{POC}}{b} + \phi_w\frac{b_w}{b} \quad \text{Eq. 8}$$

where b_{PIC} is the scattering coefficient for acid-labile particles calculated from b_b' assuming a backscattering ratio of 0.03 for coccoliths, b_{POC} is the scattering coefficient of non-acid labile particles ($b_{POC} = b_p - b_{PIC}$), and b_w is the scattering coefficient for seawater.

A model sensitivity experiment was conducted to explore the role of particle type and multiple scattering in measurements of δ. For all experiments, we assumed a value of 0.5 for $\chi_{PIC}(\pi)$ and $\chi_{POC}(\pi)$, and a value of 0.68 for $\chi_w(\pi)$[2,10]. Backscattering coefficients

for each component were parameterized from *in situ* measurements made during the Coccomix expedition. $\mathbf{M}_{22}^{w}(\pi)$ and ϕ_{w}were set to 1 and 0 respectively, as molecular scattering by water does not cause linear depolarization[10]. $\mathbf{M}_{22}^{\mathrm{PIC}}(\pi)$ was parameterized from laboratory measurements of depolarization by *Emiliania huxleyi* coccoliths (0.79; cf. Fig. 2), leaving three free-parameters in the model $\mathbf{M}_{22}^{\mathrm{POC}}(\pi)$, ϕ_{PIC}, and ϕ_{POC}. A model sensitivity analysis was performed by solving for *DoLP* using values of $\mathbf{M}_{22}^{\mathrm{POC}}(\pi)$ ranging from 0.5 to 1, and values of ϕ_{POC} and ϕ_{PIC} ranging from 0 to 0.4. Model predictions of δ for each combination of $\mathbf{M}_{22}^{\mathrm{POC}}(\pi)$, ϕ_{PIC}, and ϕ_{POC} were compared with field measurements of δ, using r^2 as a metric for the skill of each model.

Results

Scattering Measurements

Total return signal increased linearly as a function of c_{pg} for each of the serial additions, providing confidence that our measurements were within the single scattering domain (Fig. 2a). Measurements of δ showed no linear dependence on c_{pg}, providing further confidence that the experiments were conducted within the single scattering domain (Fig. 2b). δ ranged from 0.02 for *Synechococcus* to 0.26 for laboratory calcite.

Fig. 2c shows measurements of S and δ from the *E. huxleyi* acidification experiment plotted against the concentration of the stock particle suspension added to the sample chamber. Visualizing the data in this manner highlights the fractional contribution of backscatter from the acid labile particle population to the total signal S, by removing the influence of particle concentration and scattering cross-section contained in measurements of c_{pg} (Fig. 2c). The slope of S versus stock concentration decreased from 3.11E4 to 9.31E3 mV L-seawater L-stock^{-1} upon acidification, suggesting that calcite contributed to 70% of the scattered flux at

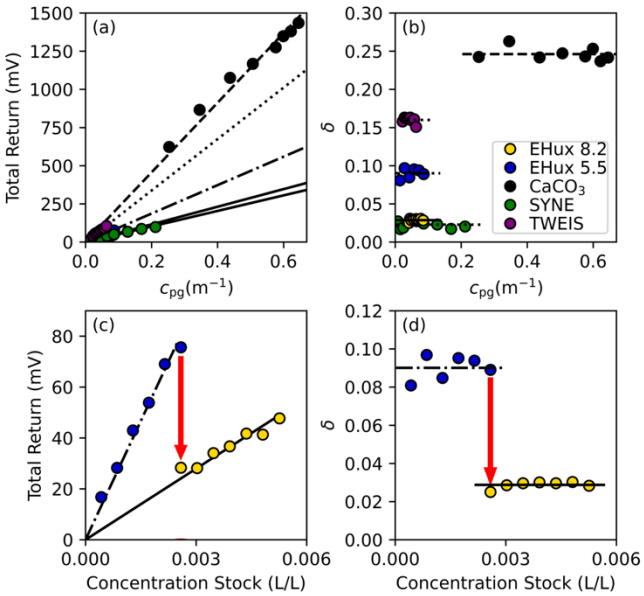

Fig. 2 Results from the near-backwards depolarization experiments. Plots of total backscattered signal (a) and d (b) versus c_{pg} for each scattering experiment [*Emiliania huxleyi* pH 8.2 (blue), *Emiliania huxleyi* pH 5.5 (green), laboratory calcite (grey), *Thalassiosira weissflogii* (purple)]. Total backscattered signal and d from the *Emiliania huxleyi* acidification experiment are additionally plotted against concentration of stock algal culture [(c) and (d) respectively]. Blue arrows highlight change in total signal and d after acidification. Regression lines (black) are forced through zero.

178.5° for the coccolithophore culture(Fig. 2c). Measurements of δ for *E. huxleyi* decreased from 0.09 to 0.03 after acidification (Fig. 2d).

Figure 3 shows values of $\mathbf{M}_{22}$ at 178.5° estimated for each particle population using Eq. 1, with the assumption that the influence of $\mathbf{M}_{12}$ on δ was negligible in the near backwards direction (e.g. $\mathbf{M}_{12} \approx 0$). Small phytoplankton species lacking mineral tests were the least depolarizing, with *Synechococcus* sp. having an $\mathbf{M}_{22}$ value of 0.96 and the acidified *Emiliania huxleyi* culture having an $\mathbf{M}_{22}$ value of 0.94 (Fig. 3). The acid labile fraction of the *Emiliania* huxleyi culture (suspended and attached coccoliths) had an $\mathbf{M}_{22}$ value of 0.79, and the

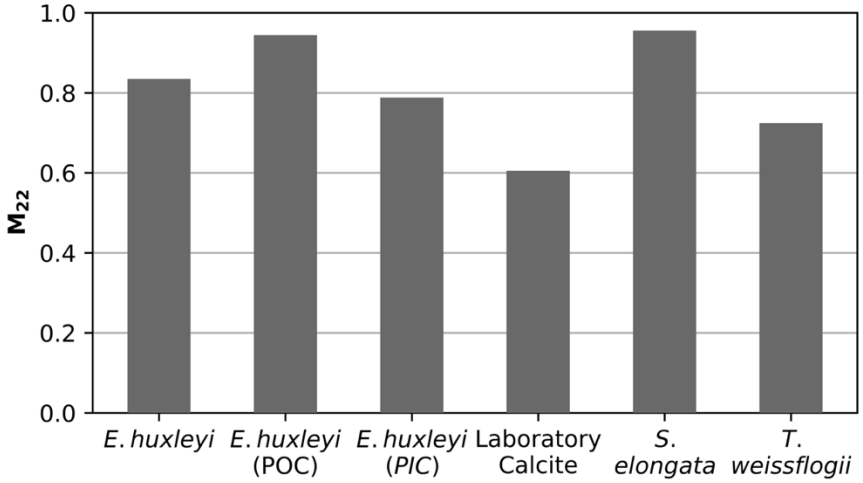

Fig. 3 Bar plot showing estimates of $\mathbf{M}_{22}$ in the near backwards direction for several different marine particles and marine particle analogs.

presence of coccoliths decreased the value of $\mathbf{M}_{22}$ for the bulk *Emiliania huxleyi* culture from 0.94 to 0.83 (Fig. 3). *Thalassiosira weissflogii* was the most depolarizing of the phytoplankton species measured here with an $\mathbf{M}_{22}$ value of 0.72. The reagent-grade calcite suspension was a stronger depolarizer than the *Emiliania huxleyi* coccolith calcite, having an $\mathbf{M}_{22}$ value of 0.60 that was substantially lower than any of the particles measured here.

Model Sensitivity Analysis

Fig. 4a shows model inputs of $\mathbf{M}_{22}^{\mathrm{POC}}(\pi)$, ϕ_{PIC}, and ϕ_{POC} plotted in three-dimensional space, with the color of each point representing the value of r^2 for that particular model solution calculated with respect to field measurements of δ. Model solutions resulting in an r^2 of less than 0.7 were excluded from the figure to improve interpretability. The model was very sensitive to the parameterization of ϕ_{POC}, and for values of ϕ_{POC} greater than 0.14, there were no model solutions that resulted in an r^2 of 0.7 or higher. The model was less sensitive to $\mathbf{M}_{22}^{\mathrm{POC}}(\pi)$ and ϕ_{PIC}, with solutions existing for the entire range of each parameter within the 0.7 r^2 criteria. Fig. 4b shows a cross-plot of $\mathbf{M}_{22}^{\mathrm{POC}}(\pi)$ and ϕ_{PIC} corresponding to the optimum model solution (as determined from the maximum in r^2) for each value of ϕ_{POC}. Optima in ϕ_{PIC} and $\mathbf{M}_{22}^{\mathrm{POC}}(\pi)$ displayed an inverse relationship, with ϕ_{PIC} decreasing as a function of ϕ_{POC} and $\mathbf{M}_{22}^{\mathrm{POC}}(\pi)$ increasing as a function of ϕ_{POC} (Fig. 4b). Changes in ϕ_{POC} were compensated for by corresponding changes ϕ_{PIC} and $\mathbf{M}_{22}^{\mathrm{POC}}(\pi)$ for values of ϕ_{POC} between 0 and 0.1, resulting in a fairly stable r^2 of ~0.9 (Fig. 4a,b). For values of ϕ_{PIC} greater than 0.1, optimum values of ϕ_{PIC} and $\mathbf{M}_{22}^{\mathrm{POC}}(\pi)$ were constrained to their respective minimum and maximum values, resulting in a rapid decrease of r^2 with increasing ϕ_{POC}.

Discussion

Laboratory measurements of particle linear depolarization presented here suggest that the value of $\mathbf{M}_{22}$ for marine particles varies as a complex function of particle composition and morphology, and that spatial gradients in $\mathbf{M}_{22}$ can be detected using oceanographic lidar measurements of δ. These results are consistent with recent oceanographic lidar studies that have attributed spatial patterns in δ to shifts in particulate $\mathbf{M}_{22}$ resulting from differences in the shape[8] and composition[7,11] of the particle population. However, $\mathbf{M}_{22}$ did not appear to be strongly driven by any single particle intensive parameter, suggesting that

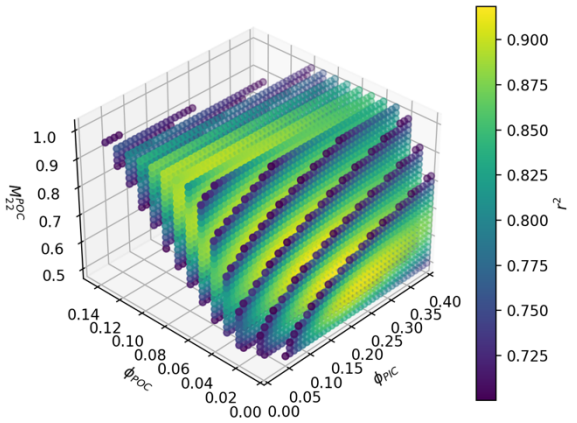

Fig. 4 Three-dimensional plot showing free parameters from Eq. 7 and 8 with the colormap depicting r^2 for each model run.

the behavior of $\mathbf{M}_{22}$ may be too complex to be useful for deriving bulk particle parameters from lidar measurements of δ. For instance, $\mathbf{M}_{22}$ was not useful for discriminating between spherical, decalcified *Emiliania huxleyi* cells and rod-shaped *Synechococcus sp.* cells, suggesting that deviations from sphericity played a negligible role in determining $\mathbf{M}_{22}$ for small, low refractive index phytoplankton. Values of $\mathbf{M}_{22}$ for high refractive index, birefringent calcite particles were elevated relative to similarly size phytoplankton cells, suggesting that $\mathbf{M}_{22}$ could be a useful metric for particle composition. However, laboratory prepared calcite particles were stronger depolarizers than similarly sized coccoliths, highlighting the complicating effect of particle morphology on efforts to extract particle compositional information from measurements of $\mathbf{M}_{22}$. Furthermore, if $\mathbf{M}_{22}$ was a useful proxy for particle bulk refractive index, we would have expected *Emiliania huxleyi* to be a stronger depolarizer than *Thalassiosira* due to the increased refractive index of calcite coccospheres relative to silica diatom tests. This was not the case, as *Thalassiosira* was more depolarizing than even a pure suspension of coccoliths.

In recent years, lidar retrievals of b_{bp} have been developed for the CALIOP spaceborne lidar instrument that use measurements of column-integrated cross-polarized backscatter and an assumed value for particle depolarization (δ_p) to estimate $\beta_p(\pi)$[12]. δ_p is commonly parameterized as a linear function of K_d ($\delta_p \approx 2K_d$), an assumption that is based on an empirical relationship between airborne lidar retrievals of K_d and δ_p derived from lidar measurements performed during the SABOR and NAAMES campaigns[13]. This fortuitous result suggests that changes in K_d are compensated for by changes in δ_p, and that independent retrievals of K_d may not be necessary for retrieving estimates of b_{bp} from CALIOP [14]. The measurements presented here suggest that this empirical relationship may be partially driven by shifts from small phytoplankton with low values of δ_p in relatively clear, oligotrophic regions of the ocean to large bloom forming species with higher values of δ_p in productive regions with elevated values of K_d. In Behrenfeld, et al. [12] and Lacour, et al. [15], δ_p was constrained to 0.3 for regions where K_d was greater than 0.15. The highest value of δ_p measured here was 0.25 for suspended laboratory calcite, with a lower value of 0.16 for the most depolarizing phytoplankton species (*Thalassiosira*). This suggests that a lower value of δ_p may be a more appropriate cutoff for CALIOP measurements of b_{bp}, and that the $\delta_p \approx 2K_d$ assumption required to neglect the K_d and δ_p terms in CALIOP b_{bp} retrievals may not be appropriate for regions where K_d leads to an overestimate of δ_p. This could account for the tendency of CALIOP to underestimate b_{bp} in regions of strong backscattering (see the supplementary information for Bisson, et al. [14]).

The model results presented here suggest that shifts in the relative contribution of particulate versus molecular scattering can play a dominant role in controlling patterns in lidar measurements of δ from bulk seawater.

This was the case for the Coccomix expedition, where a single particle model (i.e. an equivalent value of $\mathbf{M}_{22}$ for both PIC and POC) could reproduce up to 85% of the variability in δ. Within the coccolithophore bloom, correlations between δ and b_b'/b_b were driven predominantly by a strong covariation between the concentration of suspended calcite and the relative contribution of particulates to total backscattering. Had we encountered waters where measurements of b_{bp} become decoupled from b_b', the relationship between δ and b_b'/b_b would likely have deteriorated as b_{bp} became dominated by organic particles.

Previous polarized oceanographic lidar studies have struggled to separate the effects of single and multiple scattering on δ[7,8]. For instance, a recent study by Schulien, et al. [8] used the ratio of δ to b_{bp} to account for the particle concentration dependence of multiple scattering on δ. However, the ratio of δ to b_{bp} is driven primarily by the relative contribution of particulate versus molecular scattering. Furthermore, multiple scattering is a depth dependent process, and both the particle concentration and the range to the measurement must be considered to correct for its effects. The model presented here provides a framework that can be used to account for shifts in particle versus molecular scattering and to account for depolarization resulting from multiple scattering. This framework could be particularly useful for High-Spectral Resolution Lidar (HSRL) measurements, where the particulate and molecular contributions to δ can be measured directly, eliminating the need for *in situ* measurements of b_{bp} and assumptions about a particle scattering phase function.

Despite being predictive of δ throughout much of the Coccomix expedition, a single particle model of depolarization does not reproduce the bifurcation in the relationship between δ and bz that occurred in the small region of the Coccomix expedition where backscattering became uncoupled from scattering by calcite[7]. The model suggests that increased depolarization by calcite in the forward direction and an increase in particulate $\mathbf{M}_{22}$ along the coast can partially explain this bifurcation. However, these effects were subtle, and increased the explained variance from 85% to 92%.

Conclusions

The results presented here show that $\mathbf{M}_{22}$ for marine particles varies as a function of particle composition and morphology, but that the behavior of $\mathbf{M}_{22}$ may be too complex to retrieve these properties from lidar profiles of δ. This finding has important implications for satellite lidar backscatter measurements, as retrieval algorithms rely on the predictable behavior of δ_p to retrieve estimates of b_{bp} Patterns in field measurements of δ were primarily driven by shifts in the contribution of particulate vs. molecular scattering as well as the influence of multiple forward scattering. The model framework presented here represents a useful framework for untangling the contributions of single and multiple scattering to the lidar depolarization ratio. δ was found to be minimally influenced by differences in the forward scattering depolarization parameter. These results suggest that δ is a poor metric for quantifying particle type, but that profiles of δ may provide a robust technique for estimating the total scattering coefficient[16].

References

1 Jamet, C. *et al.* Going Beyond Standard Ocean Color Observations: Lidar and Polarimetry. *Frontiers in Marine Science* **6**, 251 (2019).

2 Schulien, J. A., Behrenfeld, M. J., Hair, J. W., Hostetler, C. A. & Twardowski, M. S. Vertically-resolved phytoplankton carbon and

net primary production from a high spectral resolution lidar. *Optics Express* **25**, 13577-13587 (2017).
3 Gimmestad, G. G. Reexamination of depolarization in lidar measurements. *Applied optics* **47**, 3795-3802 (2008).
4 van de Hulst, H. C. Light scattering by small particles. (1957).
5 Vasilkov, A. P. *et al.* Airborne polarized lidar detection of scattering layers in the ocean. *Applied Optics* **40**, 4353-4364, doi:10.1364/AO.40.004353 (2001).
6 Zege, E. P. & Chaikovskaya, L. I. Polarization of multiply scattered lidar return from clouds and ocean water. *JOSA A* **16**, 1430-1438 (1999).
7 Collister, B. L., Zimmerman, R. C., Hill, V. J., Sukenik, C. I. & Balch, W. M. Polarized lidar and ocean particles: insights from a mesoscale coccolithophore bloom. *Applied Optics* **59**, 4650-4662 (2020).
8 Schulien, J. A. *et al.* Shifts in Phytoplankton Community Structure Across an Anticyclonic Eddy Revealed From High Spectral Resolution Lidar Scattering Measurements. *Frontiers in Marine Science* **7**, 493 (2020).
9 Dionisi, D., Brando, V. E., Volpe, G., Colella, S. & Santoleri, R. Seasonal distributions of ocean particulate optical properties from spaceborne lidar measurements in Mediterranean and Black sea. *Remote Sensing of Environment* **247**, 111889 (2020).
10 Zhang, X., Hu, L. & He, M.-X. Scattering by pure seawater: effect of salinity. *Optics Express* **17**, 5698-5710 (2009).
11 Collister, B. L., Zimmerman, R. C., Sukenik, C. I., Hill, V. J. & Balch, W. M. Remote sensing of optical characteristics and particle distributions of the upper ocean using shipboard lidar. *Remote Sensing of Environment* **215**, 85-96 (2018).
12 Behrenfeld, M. J. *et al.* Space-based lidar measurements of global ocean carbon stocks. *Geophysical Research Letters* **40**, 4355-4360 (2013).
13 Behrenfeld, M. J. *et al.* Global satellite-observed daily vertical migrations of ocean animals. *Nature* **576**, 257-261, doi:10.1038/s41586-019-1796-9 (2019).
14 Bisson, K. M., Boss, E., Werdell, P. J., Ibrahim, A. & Behrenfeld, M. J. Particulate Backscattering in the Global Ocean: A Comparison of Independent Assessments. *Geophysical Research Letters* **48**, e2020GL090909, doi:https://doi.org/10.1029/2020GL090909 (2021).
15 Lacour, L., Larouche, R. & Babin, M. In situ evaluation of spaceborne CALIOP lidar measurements of the upper-ocean particle backscattering coefficient. *Optics Express* **28**, 26989-26999 (2020).
16 Hoge, F. *et al.* Airborne lidar detection of subusrface oceanic scattering layers. *Appl. Opt.* **27**, 39969-33977 (1988).